Changing inputs of continental and submarine weathering sources of Sr to the oceans during OAE 2

Lucien Nana Yobo[1], Alan D. Brandon[1], Chris Holmden[2], Kimberly V. Lau[3], and James Eldrett[4]

[1]Department of Earth and Atmospheric Sciences, University of Houston, Houston TX
[2]Department of Earth Science, University of Saskatchewan, Saskatoon Canada
[3]Department of Geosciences and Earth and Environmental Systems Institute, The Pennsylvania State University, University Park PA
[4]Shell International Exploration and Production, the Netherlands

Abstract

Ocean anoxic events (OAE) are characterized by increased organic content of marine sediment on a global scale with accompanying positive excursions in sedimentary organic and inorganic $\delta^{13}C$ values. To sustain the increased C exports and burial required to explain the C isotope excursion, increased supplies of nutrients to the oceans are often invoked during ocean anoxic events. The potential source of nutrients in these events is investigated in this study for Oceanic Anoxic Event 2, which spans the Cenomanian-Turonian boundary. Massive eruptions of one or more Large Igneous Provinces (LIPs) are the proposed trigger for OAE 2. The global warming associated with volcanogenic loading of carbon dioxide to the atmosphere has been associated with increased continental weathering rates during OAE 2, and by extension, enhanced nutrient supplies to the oceans. Seawater interactions with hot basalts at LIP eruption sites can further deliver ferrous iron and other reduced metals to seawater that can stimulate increased productivity in surface waters and increased oxygen demand in deep waters. The relative importance of continental and submarine weathering drivers of expanding ocean anoxia during OAE 2 are difficult to disentangle.

In this paper, a box model of the marine Sr cycle is used to constrain the timing and relative magnitudes of changes in the continental weathering and hydrothermal Sr fluxes to the oceans during OAE 2 using a new high-resolution record of seawater $^{87}Sr/^{86}Sr$ ratios preserved in a marl-limestone succession from the Iona-1 core collected from the Eagle Ford Formation in Texas. The results show that seawater $^{87}Sr/^{86}Sr$ ratios change synchronously with Os isotope evidence for the onset of massive LIP volcanism 60 kyr before the positive C isotope excursion that traditionally marks the onset of OAE 2. The higher temporal resolution of the seawater Sr isotope record presented in this study warrants a detailed quantitative analysis of the changes in continental weathering and hydrothermal Sr inputs to the oceans during OAE 2. Using an ocean Sr box model, it is found that increasing the continental weathering Sr flux by ~1.8-times captures the change in seawater $^{87}Sr/^{86}Sr$ recorded in the Iona-1 core. The increase in the continental weathering flux is smaller than the threefold increase estimated by studies of seawater Ca isotope changes during OAE 2, suggesting that hydrothermal forcing may have played a larger role in the development of ocean anoxic events than previously considered

1. Introduction

Ocean Anoxic Events (OAE) are identified in the rock record by elevated concentrations of organic matter in marine sediments and positive shifts in sedimentary $\delta^{13}C$ values, a signal major perturbation to the Earth's exogenic C cycle from increased organic carbon burial (Schlanger and Jenkyns 1976; Sageman et al., 2006). One of the most studied examples is Ocean Anoxic Event 2 (OAE 2) spanning the Cenomanian-Turonian boundary (CTB) in the Late Cretaceous. The duration of OAE 2 is 600,000 - 800,000 years

based on rhythmically bedded strata in the Western Interior Seaway (WIS) of North America (Sageman et al., 2006; Eldrett et al., 2015a; Jones et al., 2020). Traditionally, the length of the event is represented by the stratigraphic thickness of the positive $\delta^{13}C_{org}$ excursion (CIE) of 2 to 5‰ (Scholle and Arthur 1980; Jenkyns, 2010). Two factors contribute to increased organic carbon burial: (1) higher preservation at the sediment water interface, which is enhanced during periods of expanded bottom water anoxia in the oceans (e.g., Ostrander et al., 2017), and/or (2) increased exports of primary produced organic matter from the photic zone, which is improved during periods of increased nutrient availability in the oceans (Jenkyns, 2010 and references therein). The relative importance of these two processes for OAE 2 is a frequent subject of study and debate (Blättler et al., 2011; Pogge von Strandmann et al., 2013 Owens et al., 2018; Them et al., 2018). Climate and ocean circulation models generally invoke increased continental weathering during OAE 2 as a key global change variable (e.g., Topper et al., 2011; Monteiro et al., 2012; Baroni et al., 2014) and are parameterized with continental weathering proxy studies, notably Ca and Li isotopes, to set the magnitude of the continental weathering (Blättler et al., 2011; Pogge von Strandmann et al., 2013). However, the proposed threefold increase in continental weathering fluxes of Ca to the oceans during OAE 2 proposed by Blättler et al. (2011) was based on Ca isotope records that could not be reproduced in a follow-up study by

et al. (2015). The source and relative weight of increased supplies of nutrients to the oceans during OAE 2 is the subject of this study.

Early studies of OAE 2 (Schlanger and Jenkyns 1976; Demaison and Moore, 1980; Pedersen and Calvert, 1990) focused on climate and ocean circulation changes to explain

77 increased total organic carbon (TOC) concentrations in marine sediments, highlighting the
78 role of warmer Late Cretaceous climates and sluggish circulation may have played in the
79 preservation and burial of marine organic matter. Warmer temperatures cause increased
80 soil mineral weathering, resulting in increased weathering supplies of nutrients to the
81 oceans that could then fuel additional productivity, organic carbon export, increased
82 oxygen utilization in deep waters, and expanded bottom water anoxia–thereby leading to
83 organic carbon burial (Schlanger and Jenkyns 1976; Demaison and Moore, 1980; Pedersen
84 and Calvert, 1990). These studies, however, could not adequately account for the timing of
85 OAE 2 before the evidence began to grow for its volcanic origin.
86 Increased submarine volcanism during OAE 2 is supported by episodic increases
87 in trace metal abundances of basaltic affinity in carbonate sediments from the proto-North
88 Atlantic region (Orth et al., 1993). The metal source was initially attributed to increased
89 hydrothermal venting at mid-ocean ridges (Orth et al., 1993), but was quickly amended to
90 massive submarine eruptions of one or more Large Igneous Provinces (LIPs), particularly
91 the Caribbean Large Igneous Province (CLIP) in the eastern Pacific, which erupted near
92 the Central American Gateway to the proto-North Atlantic Ocean (Sinton and Duncan,
93 1997). A submarine volcanic trigger is further supported by a global decrease in global
94 seawater $^{87}Sr/^{86}Sr$ during OAE 2, and similar patterns for the other Cretaceous OAEs
95 (Ingram et al., 1994; Bralower et al., 1997; Jones and Jenkyns 2001; Ando et al., 2009).
96 The perturbations in the ocean Sr cycle offered a means by which the magnitude of the
97 eruptions and the volumes of seawater that interacted with hot basalt during LIP magmatic
98 activity could be assessed (Ingram and DePaolo, 1994). However, the response of the ocean
99 Sr cycle to the volcanic trigger was expected to be sluggish on account of the long modern

oceanic Sr residence time (2.5 Ma; Hodell et al., 1989), adjusted to 1.35 Myr in this study using updated continental input Sr fluxes from Peucker-Ehrenbrink and Fiske (2019). The poorly resolved record of changing seawater $^{87}Sr/^{86}Sr$ in the Late Cenomanian and early Turonian challenged the ability to more definitively determine shifts to the Sr cycle. Moreover, there were competing effects to the ocean Sr mass balance needs to be considered—most notably the higher continental weathering fluxes of Sr to the oceans that would drive the $^{87}Sr/^{86}Sr$ ratio of seawater in the opposite direction to that produced by increased volcanism on the ocean floor.

In contrast to Sr, the marine Os cycle shifted very abruptly from a continental weathering-dominated signature to a mantle-dominated signature, consistent with a massive magmatic event near the onset of OAE 2 (Turgeon and Creaser, 2008; DuVivier et al., 2014; Jones et al., 2020). With its much shorter ocean residence time (3–50 kyr; Oxburgh 2001) compared to Sr (~1.35 Myr) the eruptions could be shown to have started *ca.* 20–60 kyr before the positive CIE and the onset of OAE 2. However, the LIP-induced ocean Os cycle perturbation was so large that it completely overwhelmed any increase in continental weathering of Os to the oceans that may have also occurred in response to global warming driven by volcanogenic carbon dioxide emissions.

The relative importance of continental weathering and submarine volcanic delivery of nutrients to the oceans during OAE 2, and the time scales over which they played a role in its development, remain open questions, but can be partially constrained by strontium isotope records. This is because evolution of seawater $^{87}Sr/^{86}Sr$ reflects changes in two principle input Sr fluxes to the oceans: (1) venting of hydrothermal fluids from active submarine volcanism that deliver basaltic-derived micronutrients (Fe, Mn, Cu, Co, Zn) and

123 Sr with a modern $^{87}Sr/^{86}Sr$ ratio of ~0.7031 (Snow et al., 2005), and (2) rivers and
124 groundwater draining the continental crust that delivers the important macronutrient,
125 phosphate, to the oceans and Sr with a modern $^{87}Sr/^{86}Sr$ that has been estimated at 0.7110
126 (Palmer and Edmond 1989; Richter et al., 1992). The latter has been recently adjusted to
127 0.71040 to reflect the most recent comprehensive study of continental sources of Sr to the
128 oceans (Peucker-Ehrenbrink and Fiske, 2019) The higher $^{87}Sr/^{86}Sr$ of the continental
129 weathering input reflects the higher $^{87}Rb/^{86}Sr$ ratio of the continental crust. It's older rock
130 ages and higher Rb concentrations yield higher production rates of ^{87}Sr from radioactive
131 decay of ^{87}Rb, compared to the mantle-source region (0.7025–0.7037) that melts to produce
132 the oceanic crust (Wickman, 1948). Using simple mixing and the present-day seawater
133 $^{87}Sr/^{86}Sr$ of 0.7092 (Elderfield, 1986), modern Sr input fluxes to the oceans from
134 continental weathering and submarine weathering by hydrothermal fluids is estimated at
135 84% and 16%, respectively. The relative size of the inputs has changed over geological
136 time. Periods of increased mountain building correlate with higher $^{87}Sr/^{86}Sr$ ratios of
137 seawater while periods of rapid seafloor spreading and LIP eruptions correlate with lower
138 ratios (Palmer and Edmond 1989; Richter et al., 1992). Carbonates of igneous and
139 metamorphic origin in mountain uplift regions can also deliver large quantities of Sr to the
140 oceans with high $^{87}Sr/^{86}Sr$ ratios (Derry and France-Lanord 1996; Jacobson et al., 2002).
141 Documented decreases in carbonate $^{87}Sr/^{86}Sr$ ratios during OAE 2 suggests that
142 submarine hydrothermal inputs were a more dominant factor than increased continental
143 weathering inputs (Fig. 1; Ingram et al., 1994; Bralower et al., 1997; Jones and Jenkyns
144 2001; Snow et al., 2005). A seawater $^{87}Sr/^{86}Sr$ record for OAE 2 that is more precise and
145 of higher temporal resolution than those currently available (Fig. 2; Ando et al., 2009)

could help to quantify the relative change in the Sr inputs. To address this issue, a new high-resolution record of seawater $^{87}Sr/^{86}Sr$ ratios for OAE 2 is presented in this paper from the Iona-1 core (Eldrett et al., 2014; Minisini et al., 2017), which samples a succession of pelagic marine carbonates from the Eagle Ford Formation in Texas. A forward box model of the ocean Sr cycle is implemented in combination with a conceptual model of how continental weathering and hydrothermal inputs of Sr likely would have responded to a massive episode of LIP volcanism. The result is an estimate for the continental weathering flux increase of Sr to the oceans during OAE 2 (and by inference Ca and nutrients) that is smaller than previous estimates (Blattler et al., 2011; Pogge von Strandmann et al., 2013).

2. Geologic Setting

The Iona-1 core was drilled on a carbonate shelf at the southern gateway to the WIS in present-day southwest Texas (29°13.51'N, 100°44.49'W). The core recovered 180 m of Lower Cenomanian to Lower Coniacian marine sediment composed of marls and shales, with intermittent bentonite of the Boquillas Formation of the Eagle Ford Group (Eldrett et al., 2014). Sedimentation was slow and assumed to be relatively continuous during OAE 2 in the study setting (Eldrett et al., 2015a). An age model for the Iona-1 core was constructed from rhythmically deposited inter-bedded limestones and marlstones that were interpreted to reflect orbitally forced on sedimentation patterns and is supported by U-Pb zircon dating of bentonite beds (Eldrett et al. 2014, 2015a, 2015b; Minisini et al., 2017). The onset of the CIE in the Iona-1 core has recently been picked at 112.45 m based on the presumed first increase towards more positive $\delta^{13}C_{org}$ values (i.e., Eldrett et al., 2015a; Eldrett et al., 2017; Minisini et al., 2018; Sullivan et al. 2020). However, there is some uncertainty in the exact

placement of the start of OAE 2 CIE as the increase in $\delta^{13}C_{org}$ is subtle over a few meters reflecting the continuous sedimentation over this interval compared to other sections (i.e., Pueblo, CO, USA). This uncertainty was highlighted by Eldrett et al. (2014; 2015b) with some authors placing the start of the CIE at 110.01m (Jenkyns et al. 2017). This study follows the Jenkyns et al. (2017) placement of the onset of OAE 2 in the Iona-1 core. The interbedded marls are predominantly finely laminated and organic-rich in the lower Eagle Ford and become more bioturbated up core (Eldrett et al., 2014). Stratigraphic patterns in the traces of burrowing organisms and the diversity of benthic foraminifera documented periods of alternating oxic to dysoxic and aoxic bottom waters in the study area during OAE 2. Intervals of organic-rich laminated sediment and elevated trace metal nutrients are associated with bottom water anoxia (Eldrett et al., 2014; 2015a and Minisini et al., 2017), The depth of deposition is interpreted to be consistently below storm wave base in a restricted, sediment-starved setting (100 to 200 m depth; Eldrett et al, 2014). The decrease in initial $^{187}Os/^{188}Os$ begins ~60 kyr prior to the onset of the positive C isotope excursion that traditionally marks the base on OAE 2 and, consistent with recently published Os isotope evidence supporting the volcanic trigger hypothesis for OAE 2 (DuVivier et al., 2014, Jones et al., 2020). The carbonate fraction of the sediment is mostly original low magnesium calcite mud derived from planktic foraminifera and calcispheres. Further details on the sedimentology, stratigraphy, and hydrographic conditions can be found in Eldrett et al., (2014, 2015a, 2017) and Minisini et al. (2017).

3. Analytical Techniques

3.1 Sample dissolution

192 Samples were collected approximately every 25 cm for Sr isotope analysis in the
193 study interval of the core. The mixed limestone-marlstone-siliciclastic lithology of the
194 Iona-1 core makes it important to use an acid that will dissolve carbonate minerals
195 precipitated from seawater but will not appreciably attack and release Sr from non-
196 carbonate minerals with higher or lower $^{87}Sr/^{86}Sr$ ratios. The dissolution procedure
197 employed in this study has two sequential steps: (1) an ammonium acetate wash to remove
198 Sr from exchange sites on clays and broken mineral surfaces from grinding, and (2)
199 dissolution of the carbonate fraction of the sediment in buffered acetic acid (Bailey et al.,
200 2000).
201 In detail, 5 mL of 1 M ammonium acetate solution was added to 200 mg of rock
202 powder for 12 hours after which sample was centrifuged, the supernatant decanted, and the
203 sample rinsed three times with ultrapure water. The samples were then immersed in 5 mL
204 of 1 M buffered Optima glacial grade acetic acid for 1–2 hours at room temperature to
205 dissolve carbonate minerals. The leachate was separated from the residue by centrifugation.
206 The solution was then dried down and the acetate removed by redissolving the sample in a
207 few mL of 6 N nitric acid (HNO_3) and dried down again. This step was repeated three times
208 to ensure that acetate was decomposed. The residues were then dissolved in 0.45 N HNO_3
209 and transferred to pre-weighed acid-cleaned 50 mL centrifuge tubes. An aliquot of the
210 stock solution was used for the analysis of elemental concentrations by inductively coupled
211 plasma mass spectrometry (ICPMS) and inductively-coupled optical emission mass
212 spectrometry (ICP-OES). Another aliquot was passed through a column containing
213 Eichrom Sr Spec resin to purify Sr from Ca and other matrix elements prior to mass
214 spectrometric analysis using thermal ionization mass spectrometry (TIMS).

215

216 *3.2 Analytical techniques*

217 Major and trace element concentrations were determined by ICP-OES and ICP-MS,
218 respectively, at the University of Houston. Analytical uncertainty is generally better than
219 ±5% 1σ, monitored by repeated analysis of an internal standard. The $^{87}Sr/^{86}Sr$ ratios were
220 measured using a on a Thermo Scientific Triton Plus TIMS at the University of Houston
221 using a multi-static measurement technique adapted from a method for obtaining high
222 precision Nd isotopic ratios (Bennett et al., 2007). The measurement procedure begins with
223 a slow increase of the filament temperature during which time the Sr ion beams are located,
224 tuned, and peak-centered multiple times until a stable ^{88}Sr ion beam intensity of 6V is
225 reached. Three sets of Sr isotopic ratios were collected in each cycle (3 scans), with 10
226 cycles per block and 14 blocks per run, for a total of 420 measurements of $^{88}Sr/^{86}Sr$,
227 $^{87}Sr/^{86}Sr$ and $^{84}Sr/^{86}Sr$. Mass 85 was monitored to correct $^{87}Sr/^{86}Sr$ for ^{87}Rb interference,
228 but Rb beams were too small to warrant any significant corrections. The $^{87}Sr/^{86}Sr$ ratios
229 were corrected for instrumental mass fractionation using a $^{86}Sr/^{88}Sr$ ratio of 0.1194.

230 The external precision for $^{87}Sr/^{86}Sr$ is ±5 ppm (2σ) base on repeated measurements
231 of the SRM 987 standard yielding 0.710251± 2.951E-06 (n=20) over the course of this
232 work.

233

234 **5. Results**

235 *5.1 Elemental concentrations*

236 Trace element concentrations were used to screen the leachates for non-carbonate
237 sources of Sr by monitoring co-release of Al and Rb that are high in detrital clay minerals

but low in marine carbonates (Tribovillard et. al., 2006). The low Al concentrations (average ~200 ppm) in the leachates indicate that the ammonium acetate rinse of the sample powders and the weak acetic acid used to dissolve carbonate minerals resulted in a very minor release of Al from the samples (see supplements Table S1). The Al concentrations in the leachates are consistent with those of modern pure carbonate sediments where the main source of Al is from seawater itself (Veizer, 1983). As a point of comparison, Veizer (1983) reports 4600 ppm Al in pure marine carbonates, which is higher than concentrations measured in this study, and much lower than concentrations of ~80,000 ppm in shales. The low Al concentrations in the sample leachates is strong evidence for negligible release of Sr from non-carbonate minerals.

Manganese can also reside in metalliferous coatings on sediment grains. Although the concentration of Sr is insignificant in these coatings (Veizer, 1983), sample leachates with elevated Mn concentrations may still record seawater $^{87}Sr/^{86}Sr$ ratios. Higher Mn concentrations in carbonates deposited in the proto-North Atlantic region during OAE 2 (Pratt et al., 1991) reflect higher oceanic inventories of Mn, due to the reduction in the size of the oxic marine sink where Mn-oxides would have normally accumulated, and increased Mn fluxes from hydrothermal weathering of the LIP basalts (Orth et al., 1993; Sinton and Duncan, 1997; Snow et al., 2005). However, the Mn concentrations recorded in the carbonate fractions of the Iona-1 core are relatively low.

5.2 Sr isotopes

The carbonate $^{87}Sr/^{86}Sr$ profile in the Iona-1 core is a smoothly varying function of stratigraphic depth (Fig. 1). This meets the expectation for a sedimentary succession with

no major depositional hiatuses, for an element like Sr with a long oceanic residence time. The overall trend is one of increasing $^{87}Sr/^{86}Sr$ before OAE 2 followed by a decreasing trend in the early part of OAE 2, a period of no change in $^{87}Sr/^{86}Sr$ in the middle part of OAE 2, and a resumption of the declining trend in $^{87}Sr/^{86}Sr$ for the remainder of OAE 2. In detail, the shift from increasing to decreasing $^{87}Sr/^{86}Sr$ ratios near the onset of OAE 2 occurs at the same stratigraphic level as the decrease in $^{187}Os/^{188}Os$ ratios signaling the massive increase in LIP volcanism. The ~ 150 kyr of no change in $^{87}Sr/^{86}Sr$ occurs in a stratigraphic interval marked by the beginning of the post-volcanic rise in oceanic $^{187}Os/^{188}Os$ ratios, and the end of the peak positive shift in sedimentary $\delta^{13}C$ values (Fig. 1). Carbonate $^{87}Sr/^{86}Sr$ ratios continue to decline for ~2.5 Myr after OAE 2, until about the end of the Turonian, at which point they being to increase again.

6. Discussion

Before interpreting the $^{87}Sr/^{86}Sr$ trend in the Iona core, it is important to consider the likelihood that it genuinely reflects secular change in seawater $^{87}Sr/^{86}Sr$ during OAE 2, rather than stratigraphic changes in diagenetic or local Sr cycling effects.

6.1 Diagenetic effects

Seawater derived Sr can be difficult to extract from mixed carbonate/siliciclastic lithologies without also releasing Sr from the detrital silicates. The ion exchange wash and weak acetic acid dissolution used in this study appears to have successfully targeted the release of Sr from carbonate minerals, based on the low Al concentrations in the acid leachates. A more difficult problem is the diagenetic transfer of silicate derived Sr into new carbonate mineral growth. However, there are a number of factors to consider that make

284 recrystallization of the carbonates in the Iona core potentially less of a problem than in
285 carbonate sediments from other settings. Firstly, the source of the carbonate mud is pelagic
286 calcifiers (i.e. foraminifera and coccolithophores) that produce low magnesium calcite
287 (LMC), which is the most diagenetically stable calcium carbonate polymorph. Secondly,
288 the sediments have low permeability, and the observed carbonate cements have been
289 interpreted to have precipitated in close diagenetic system (Eldrett et al., 2015b., Minisini
290 et al. 2017). Accordingly, any cements that formed would likely re- incorporate seawater-
291 derived Sr released to the pore fluids. Oxygen isotopes in the Iona-1 core show no obvious
292 evidence for recrystallization of carbonates, such as low $\delta^{18}O$ values indicative of higher
293 temperatures encountered during deep burial, or meteoric waters (Eldrett et al., 2015b).
294 The bulk carbonate $\delta^{13}C$ and $\delta^{18}O$ values in the Iona-1 core are similar to well preserved
295 calcite tests of calcite foraminifera reported in other locations of the WIS (Eldrett et al.,
296 2015b and references therein). Hence, the $^{87}Sr/^{86}Sr$ ratios in the carbonate fractions were
297 likely not altered by diagenetic processes. Hence it is concluded that the $^{87}Sr/^{86}Sr$ in the
298 carbonate fractions measured here were unlikely to be reset by post-depositional diagenetic
299 processes.

300 *6.2 Local Sr cycling effects*

301 Even in cases where diagenetic effects are negligible and the sample dissolution
302 procedure only releases seawater-derived Sr from the samples, marine carbonates
303 deposited in epeiric seas may record $^{87}Sr/^{86}Sr$ ratios that are different from the global ocean
304 due to circulation restrictions and local Sr cycling. The study setting is located at the
305 southern gateway to the WIS—an epeiric seaway that did not support a typical mid-
306 Cretaceous marine fauna (McArthur at al., 1994, Eldrett et al., 2017, Minisini et al., 2017).

307 Moreover, the WIS experienced climate oscillations that affected precipitation and
308 freshwater inputs from rivers. These changes, in turn, affected salinity patterns, water
309 column stratification and mixing in the Seaway, while longer term changes in sea level
310 could eased or restrict the flow of water over the sill at the southern and northern gateways
311 (Holmden et al., 1997a, 1997b; Cockran et al., 2003). The long length of the Seaway,
312 equivalent to the distance between the present-day Arctic and Gulf of Mexico, increases
313 the likelihood that local Sr cycling effects could be important in different parts of the
314 Seaway at different times. The Late Cenomanian eustatic sea-level rise, and the location of
315 the study setting near the southern gateway to the WIS lend support to improved circulation
316 in the southern part of the Seaway during OAE 2. As an additional consideration, the large
317 difference in the Sr concentration between seawater and river waters dictates that the
318 salinity must typically decrease to below ~15‰ before the local $^{87}Sr/^{86}Sr$ of brackish
319 seawater can begin to deviate significantly from the global ocean $^{87}Sr/^{86}Sr$ ratio (Anderson
320 et al., 1992; Holmden et al., 1997a, 1997b; Holmden and Hudson, 2003). However, some
321 forms of submarine groundwater discharge (SGD) have the potential to change seawater
322 $^{87}Sr/^{86}Sr$ ratios without any appreciable adjustments of salinity (Beck et al., 2013). A large
323 Sr flux from SGD was likely important in the Late Cretaceous WIS in South Dakota
324 (Cochran et al., 2003).
325 The role of local Sr cycling effects in the Seaway setting of the Iona-1 core is best
326 evaluated with records from nearby locales in the WIS where circulation restriction is more
327 likely—but these records do not exist. With spatially distributed records, a gradient in
328 seawater $^{87}Sr/^{86}Sr$ ratios, if present, could be used to reveal locations affected by local Sr
329 cycling and the direction of change in local seawater $^{87}Sr/^{86}Sr$ ratios compared the open

ocean ratio. Until more local/regional records are available, the only remaining option is to compare the Iona-1 record to other published records regardless of their location. To do so, the records presented here were re-normalized to the SRM 987 ratio of 0.710251 obtained in this study (Figs. 1 and 2).

All but one of the published $^{87}Sr/^{86}Sr$ records are inconsistent with the record of the Iona-1 core presented in this study. They are also inconsistent with each other (Fig. 1). Most of the published records depict higher inferred seawater $^{87}Sr/^{86}Sr$ ratio during OAE 2. The Iona-1 core record gives lower $^{87}Sr/^{86}Sr$ ratios than the LOWESS curve of seawater $^{87}Sr/^{86}Sr$ (McArthur et al., 2012). Well-preserved rudists collected from near shore deposits representing shallow water settings in the Southern Apennines during OAE 2 (Frijia and Parante, 2008) gave even higher $^{87}Sr/^{86}Sr$ ratios than the LOWESS curve. These results were interpreted to reflect Sr inputs from local rivers, implying brackish waters and salinity stratification in this setting (Frijia and Parante, 2008). The $^{87}Sr/^{86}Sr$ ratios spanning OAE 2 are also high in several Deep Sea Drilling Project Sites (DSDP) Site 511 (Falkland Plateau South Atlantic; Bralower et al., 1997), DSDP Site 258 (Naturaliste Plateau, Indian Ocean; Bralower et al., 1997), DSDP Site 551 (Goban Spur, North Atlantic; Bralower et al., 1997), and the ODP Site 763B (Exmouth Plateau, Indian Ocean; Bralower et al., 1997). The carbonates in these deposits are primarily planktonic foraminifera that appear to have been altered (cf. Bralower et al., 1997). Although the data are sparse, the $^{87}Sr/^{86}Sr$ ratios from Site 511 overlap those from the Iona-1 core immediately before OAE 2, but then shift to relatively high $^{87}Sr/^{86}Sr$ ratios in the early stages of OAE 2 before decreasing again in the latter stages. The English Chalk (McArthur et al., 1993a) has the highest $^{87}Sr/^{86}Sr$ ratios

before OAE 2 of any of the published records and a decrease in $^{87}Sr/^{86}Sr$ during OAE 2 that is broadly consistent with the Iona-1 core record offset to higher ratios.

The $^{87}Sr/^{86}Sr$ record of OAE 2 that best matches the Iona-1 core is from DSDP Site 463, a carbonate succession draping the margin of a mid-Pacific atoll (Ando et al. 2009). Although the DSDP Site 463 data are sparse in the OAE 2 interval, $^{87}Sr/^{86}Sr$ ratios are consistently lower than the other published records. Like the Iona-1 core and English Chalk, carbonate $^{87}Sr/^{86}Sr$ ratios increase before OAE 2 and decrease after the onset of OAE 2. However, the low sampling resolution of the DSDP Site 463 record does not permit a confirmation of the 150 kyr interval of no change in seawater $^{87}Sr/^{86}Sr$ in the middle of OAE 2 that is present in the Iona-1 core record. To reconcile Site 463 with other published records, Ando et al. (2009) conceded that sections of the record could be shifted to lower $^{87}Sr/^{86}Sr$ ratios due to carbonate recrystallization in the presence of altered pore waters generated by water-rock interactions with basaltic volcanic rocks located at the base of the carbonate succession. The implications being that Sr bearing fluids may have migrated upwards through the sediment as a result of compaction and/or heating from below (Richter and Liang, 1993). However, the similarly low $^{87}Sr/^{86}Sr$ ratios found in the Iona-1 core in the WIS, which is not underlain by basaltic volcanic rocks, indicate that these interactions were either inconsequential or did not happen at Site 463. Neither does it seem likely that Sr released into pore fluids from altered volcanic ash beds is responsible for lowering the carbonate $^{87}Sr/^{86}Sr$ ratios in the Iona-1 core, as it would have to then be concluded that the similarities between the two records are a coincidence.

In summary, local Sr cycling effects could be responsible for the poor reproducibility observed in some shallow water carbonate records of changing $^{87}Sr/^{86}Sr$

ratios during OAE 2 (cf. Frijia and Parante 2008). Other $^{87}Sr/^{86}Sr$ records may have been altered during diagenesis (McArthur et al., 1993a; Bralower et al., 1997). Contamination of seawater derived Sr from lithogenic Sr released from detrital silicates has been recognized as problem hampering accurate reconstructions of seawater $^{87}Sr/^{86}Sr$ ratios using bulk carbonate sediments for a long time, which is why carbonate fossils have been used instead (e.g., Veizer, 1983; Edwards et al., 2015; El Meknassi et al., 2018). If investigated in a systematic way in future studies, local Sr cycling effects can provide important information on circulation patterns and the general hydrography of epeiric seas like the WIS during OAE 2. At present, the reliability of the promising similarities between the $^{87}Sr/^{86}Sr$ records of the Iona-1 core and DSDP Site 463 core to gauge the likelihood that the more detailed record of the Iona-1 core accurately records changes in the $^{87}Sr/^{86}Sr$ ratio of the oceans during OAE 2.

6.3 Key patterns of change in seawater $^{87}Sr/^{86}Sr$ during OAE 2

LIP eruptions have been implicated to cause decreases to lower seawater $^{87}Sr/^{86}Sr$ ratios in the Cretaceous, including OAE 2 (Ingram et al., 1994; Jones and Jenkyns, 2001), but this is the first time that a decrease in carbonate $^{87}Sr/^{86}Sr$ ratios has been shown to occur synchronously with the decrease in seawater initial $^{187}Os/^{188}Os$ ratios. This suggests a casual effect where the hydrothermal weathering of the LIP basalts delivered large quantities of Sr to the oceans, beginning *ca.* 60 kyr before the onset of OAE 2 (Fig. 1). Continental weathering is assumed to have also increased the flux of Sr to the oceans during OAE 2, but its effect on the seawater $^{87}Sr/^{86}Sr$ ratio is likely to be masked by the stronger change in Sr inputs from submarine volcanism. However, when the Os isotopes begin to

shift back to baseline, indicating waning of submarine volcanism, the continental weathering flux of Sr may become visible again in the seawater $^{87}Sr/^{86}Sr$ record. The stratigraphic interval of arrested change in the carbonate $^{87}Sr/^{86}Sr$ record may signal the timing of this effect. These nuances in the seawater $^{87}Sr/^{86}Sr$ record are used to estimate the sizes of the continental and hydrothermal input Sr-flux changes to the oceans during OAE 2 using an ocean Sr box model.

A unique solution for any change in seawater $^{87}Sr/^{86}Sr$ is difficult to determine. For example, an increase in seawater $^{87}Sr/^{86}Sr$ can be produced by: (1) increasing the continental weathering Sr flux, (2) decreasing the hydrothermal Sr flux, or (3) increasing the $^{87}Sr/^{86}Sr$ ratio of the continental weathering flux. Accordingly, there are multiple ways to produce every change in seawater $^{87}Sr/^{86}Sr$ and they are not mutually exclusive. Accordingly, a conceptual model with additional geological constraints is needed to implement the box model. For example, an invariant hydrothermal flux during OAE 2 is not in accordance with the evidence for submarine volcanism during the event and can therefore be ruled out (Turgeon and Creaser 2008; Jenkyns, 2010; DuVivier et al., 2014; Sullivan et al., 2020). Reducing the continental weathering flux of Sr can generate the declining trend in seawater $^{87}Sr/^{86}Sr$ ratio during OAE 2, but this is inconsistent with global warming predicted from volcanic outgassing of carbon dioxide, which should have accelerated continental weathering (Snow et al., 2005; Jenkyns, 2010). The Sr flux input from hydrothermal and continental weathering likely both increased in the early stages of OAE 2, as discussed above, but the hydrothermal inputs must have increased more to produce the early declining trend in seawater $^{87}Sr/^{86}Sr$. It is reasoned that any further changes in the apportioning of the Sr flux inputs in the midst of OAE 2 should also lead to

421 changes in the slope of the $^{87}Sr/^{86}Sr$ trend with time, if the relative flux change in one input
422 is not overwhelmed by the relative flux change in the other.

423 As indicated above, there are two subtle changes of slope in the seawater $^{87}Sr/^{86}Sr$
424 trend with time that occur in the middle of OAE 2 signaling the first time since the begining
425 of the eruptions, that the continental weathering Sr flux is no longer completely dominated
426 by the hydrothermal Sr flux. The first inflection point occurs at the 105 m depth (labeled
427 A in Fig. 1) where massive volcanism ends or dramatically declines, as indicated by the
428 rise in $^{187}Os/^{186}Os$ ratios (Fig. 1). Above this level the $^{187}Os/^{188}Os$ ratio of seawater steadily
429 increases, favoring a shift to greater relative inputs of Os from continental weathering. The
430 second, stratigraphically higher inflection point occurs at 100 m depth (labeled B in Fig.
431 1), coincident with the termination or dramatic decrease of organic carbon burial in ocean
432 sediments, as signaled by the start of the return to pre-excursion $\delta^{13}C_{org}$ As increased
433 organic carbon burial in the oceans during OAE 2 is at least partly tied to increased
434 continental weathering inputs of nutrients needed to fuel additional productivity, the
435 decline in $\delta^{13}C_{org}$ values at the end of OAE 2 is a logical place to expect continental flux
436 perturbation.

437 Two additional constraints underpin the modeling. Firstly, after terminating the
438 continental weathering Sr flux perturbation terminates at 105 m (label A Fig. 1), the
439 $^{87}Sr/^{86}Sr$ ratio of seawater must continue to steadily decline for another 1 million year (Fig.
440 1) after OAE 2. The second constraint relates to the rising trend in seawater $^{87}Sr/^{86}Sr$ before
441 OAE 2, (124–114 m), representing ~ 500 kyr of time before the eruption of the LIP that
442 drove seawater $^{87}Sr/^{86}Sr$ in the opposite direction. Whether the rising trend before the LIP
443 eruptions was due to increased continental weathering inputs, decreased hydrothermal

444 inputs, or some combination of the two cannot be uniquely determined. And yet the choice
445 made here could affects the outcome of the forward modeling, specifically the relative
446 magnitudes of the modeled Sr flux increases from continental weathering and hydrothermal
447 venting during OAE 2. As it is not known which scenario is correct, two forward models
448 of seawater $^{87}Sr/^{86}Sr$ changes during OAE 2 are produced, resulting in two estimates of the
449 change in the continental weathering input of Sr to the oceans during OAE 2 (Fig. 3A, B).
450
451 *6.4 Estimating Sr flux perturbations to the oceans during OAE 2*
452 A box model is used to quantify the perturbations of the ocean Sr cycle that can
453 account for the observed changes in seawater $^{87}Sr/^{86}Sr$ ratio during OAE 2. A coupled Sr
454 mass and Sr-isotope mass balance approach is used here. Parameters are based on modern
455 values, adjusted for the Cretaceous based on available constraints that are described in
456 detail below.
457 The time dependent change in the inventory of Sr in the oceans is represented by
458 Eq. 1,

459 $$\frac{dN_{Sr}}{dt} = J_{riv} + J_H + + J_{dia} - J_{ppt} \qquad (1)$$

460 where N_{Sr} represents moles of Sr in the oceans and J_{riv}, J_H, J_{dia} and J_{ppt} are the riverine
461 (i.e. continental weathering), hydrothermal, diagenetic and carbonate precipitation fluxes,
462 respectively. The corresponding $^{87}Sr/^{86}Sr$ ratio of the seawater is given by Eq. 2,

463 $$\frac{dR_{SW}^{Sr}}{dt} = \frac{J_{riv}^{Sr}\left(R_{riv}^{Sr} - R_{SW}^{Sr}\right) + J_H^{Sr}\left(R_H^{Sr} - R_{SW}^{Sr}\right) + J_{Dia}^{Sr}\left(R_{Dia}^{Sr} - R_{SW}^{Sr}\right)}{N_{Sr}} \qquad (2)$$

464 where R_{SW}^{Sr} represents the $^{87}Sr/^{86}Sr$ ratio of the ocean Sr reservoir and R_{riv}^{Sr}, R_H^{Sr}, and R_{Dia}^{Sr}
465 are the $^{87}Sr/^{86}Sr$ ratios of the riverine, hydrothermal, and diagenetic Sr inputs, respectively.

Initial $^{87}Sr/^{86}Sr$ ratios and Sr input fluxes were obtained from present-day estimates (Table 2) with several adjustments that are explained below. The output flux of Sr depends on the N_{Sr} and is parameterized using a first-order rate constant calculated from the initial conditions. As with many box models, steady state is assumed prior to running the model.

Two revisions were made to the modern ocean Sr budget to account for differences in the Late Cretaceous Sr cycle. First, the $^{87}Sr/^{86}Sr$ ratio of all continental sources of Sr (the riverine flux, submarine groundwater discharge, and terrestrial volcanic sources are combined into the J_{riv}) was adjusted from the present-day ratio of 0.71040 down to 0.70791 in order to achieve a steady-state $^{87}Sr/^{86}Sr$ ratio for Late Cretaceous seawater representing a period of unchanging $^{87}Sr/^{86}Sr$ ratios at the base of the study core (Fig. 1). This is not meant to imply that the ocean Sr cycle was truly in steady state at this time, but rather, to give a set of initial conditions against which changes in ocean Sr cycling that occur above this level in the core can be compared to. Second, the background hydrothermal flux was increased by 65% in accordance with reconstructions of higher Cretaceous seafloor spreading rates compared to the modern (Berner 1994). It is assumed that Late Cretaceous N_{Sr} was comparable to the modern reservoir of size of 1.25×10^{17} moles of Sr, which gives a residence time of 1.35 Myr (Table 2). Multiple limes of evidence suggest that the Sr concentration of seawater was higher in the Late Cretaceous than today (Steuber and Veizer, 2002; Coogan 2009; Antonelli et al., 2017; Akhtar et al., 2020; Zhang and DePaolo, 2020) and consequently, the oceanic Sr residence time was longer than today. To investigate the sensitivity of the model results to higher seawater Sr concentration, the model is run for

various Sr reservoir size up to 5-times larger than modern, which corresponds to a residence time >5 Myr.

The ocean Sr cycle is forced by changing one or both of the two largest input Sr fluxes to the oceans, J_{riv} and J_H. A step-change in either flux causes an initially relatively quick change in the $^{87}Sr/^{86}Sr$ ratio of seawater that slows exponentially with time as it approaches the steady state $^{87}Sr/^{86}Sr$ ratio within five residence times (~7 Myr). Because OAE 2 lasts for maximum of ~800 kyr, none of the flux perturbations employed to simulate the trend in seawater $^{87}Sr/^{86}Sr$ ratio during OAE 2 occurs long enough for the ocean Sr cycle to reach steady state.

The simulations show that the continental weathering flux of Sr to the oceans increased by 1.8-times the value of the modern Sr flux of $66.1X10^9$ moles/y (Table 2). depending on how the rising trend in seawater $^{87}Sr/^{86}Sr$ is treated before OAE 2 is treated as discussed in Section 6.3 (Fig. 3). The slightly lower estimate is the result of treating the increasing trend in seawater $^{87}Sr/^{86}Sr$ before OAE 2 as the effect of increasing continental weathering inputs of Sr to the oceans and constant hydrothermal inputs. The slightly higher estimate treats the increasing trend in seawater $^{87}Sr/^{86}Sr$ before OAE 2 as the effect of decreasing hydrothermal fluxes of Sr to the oceans and constant continental weathering inputs. These results are effectively the same and show that how the increase in $^{87}Sr/^{86}Sr$ before OAE 2 is treated does not significantly affect the result. On the other hand, it is important to bear in mind that the model results only consider changes in the input fluxes of Sr to the oceans and make the assumption that the $^{87}Sr/^{86}Sr$ ratio of the continental weathering flux was constant. Considering that OAE 2 occurred near the peak of the Late Cenomanian transgression, if the flux-weighted average $^{87}Sr/^{86}Sr$ ratio of the continental

511 weathering flux changed during OAE 2, it would have likely increased due to the drowning
512 of carbonate platforms with low $^{87}Sr/^{86}S$ ratios. If this is correct, then the increase in the
513 continental weathering flux of Sr to the oceans would have been lower than the results
514 shown in Fig. 3.

515 By considering the sensitivity of the model results to differences in initial
516 conditions, it is unlikely that the continental weathering flux of Sr to the oceans during
517 OAE 2 is underestimated. Moreover, assuming that the increase in continental Sr flux
518 scales proportionately to the continental Ca, Li and nutrient fluxes, the smaller continental
519 weathering response to the LIP eruption suggested here—compared to previous estimates
520 of a threefold increase (Blättler et al., 2011; Pogge on Strandmann et al., 2013)— has
521 important implications for the ocean eutrophication model of OAE 2, where the expansion
522 of ocean anoxia and increased burial of organic carbon is largely driven by increased
523 productivity that is stimulated by increased continental weathering supplies of nutrient
524 phosphate to the oceans (see below). The lower continental weathering response elevates
525 the importance of other contributing factors to anoxia, such as the role played by reduced
526 metals and gases to the oceans from the LIP eruptions (Snow and Duncan, 1997), the
527 paleogeography and circulation of the proto-North Atlantic nutrient trap and its
528 surrounding epeiric seas (Trabucho-Alexandre et al., 2010), positive feedbacks related to
529 P-recycling efficiency (Ingall and Jahnke, 1994), and more organic carbon burial due less
530 efficient remineralization in anoxic bottom waters (increased preservation).

531 The Iona-1 record shows decreasing seawater $^{87}Sr/^{86}Sr$ ratios continuing after the
532 cessation of OAE 2. Because the forcing from excess Sr input from LIP volcanism and the
533 continental weathering flux perturbation was removed near the end of OAE 2, the

534 expectation is that seawater $^{87}Sr/^{86}Sr$ ratio of seawater should eventually reverse and reach
535 to a new higher steady-state $^{87}Sr/^{86}Sr$ ratio after about five residence time. Instead, it
536 continues falling with no evidence of change at the end of OAE 2. This pattern can be
537 modeled to produce a new steady state by decreasing the hydrothermal input Sr flux to the
538 oceans at the end of the peak interval of the CIE or by decreasing the continental weathering
539 Sr flux. The latter is favored here, because excess hydrothermal inputs of Sr to the oceans
540 is expected to end in concert with the relaxation of initial $^{187}Os/^{186}Os$. One other possibility
541 is that the $^{87}Sr/^{86}Sr$ ratio of continental weathering decreased around this time. This would
542 require large changes in the types of continental rocks exposed to weathering, which is
543 unlikely on short time scales. It is even less likely that the hydrothermal Sr flux would
544 change without first signaling a change in seawater initial $^{187}Os/^{186}Os$, so a reduction in the
545 continental weathering input is the favored explanation.

546 Published records show that the declining trend in seawater $^{87}Sr/^{86}Sr$ continued for
547 2.5 Myr until about the end of the Turonian (Fig. 2). Thereafter, $^{87}Sr/^{86}Sr$ ratios rise steeply
548 for the next ~25 Myr, consistent with a first order decrease in ridge-crest hydrothermal
549 activity in the oceans (Berner, 1994). The increasing trend in seawater $^{87}Sr/^{86}Sr$ is the
550 dominant trend over the Late Cretaceous period, which continues into the Cenozoic
551 (Vérard et al., 2015). It is therefore the intervals of decreasing seawater $^{87}Sr/^{86}Sr$ that are
552 anomalous when considering the broader time frame (Jones and Jenkyns, 2001). This is
553 evidence that continental weathering Sr flux inputs were either much smaller in the Late
554 Cretaceous than they are today, or that hydrothermal Sr flux inputs were much larger
555 (Ingram et al., 1994). These broader findings are mirrored in this more detailed study of
556 ocean Sr cycle changes during OAE 2.

6.5. Additional considerations regarding ocean eutrophication and residence time

The ocean eutrophication model (Schlanger and Jenkyns 1976; Demaison and Moore, 1980; Pedersen and Calvert, 1990) predates the broader understanding of OAE 2 that has emerged in recent years. Most notably, it has been established that eruptions of one or more LIPs triggered the event (Turgeon and Creaser, 2008; DuVivier et al., 2014; Sullivan et al., 2020), that the small and relatively secluded proto-North Atlantic Ocean functioned as nutrient trap (Trabucho-Alexandre et al., 2010), that records of environmental changes during OAE 2 from the proto-North Atlantic ocean and surrounding seas may give a distorted picture of the global change impacts, and that the Caribbean LIP erupted near the main oceanic gateway to the proto-North Atlantic in Central Americas (Fig. 1). The latter could expedite the delivery of: (1) trace metal nutrients to the proto-North Atlantic, most notably iron, which limits primary productivity even in nutrient replete regions of the modern oceans (Leckie et al., 2002; Monteiro et al., 2012), and (2) anoxic, intermediate depth waters to the proto-North Atlantic that could increase the preservation of exported organic matter from the photic zone and its burial in the proto-North Atlantic region, while over time increasing productivity and anoxia through the positive feedback involving sedimentary phosphorous recycling (Ingall et al., 1993). In other words, the eruption of Caribbean LIP would have increased organic carbon burial in the proto-North Atlantic basin without any increase in continental weathering rates during OAE 2. Additional considerations are needed to explain the geographic variability and magnitude of the OAE 2 C isotope excursion, which cannot simply be attributed organic carbon burial (Owens et al., 2018).

580 The modeled excess of hydrothermally sourced Sr to the oceans can be converted
581 to implied volumes of new oceanic crust produced by the LIP eruption(s) that triggered
582 OAE 2. For this, the modern estimated ridge-crest hydrothermal Sr exchange flux of 6 x
583 10^8 mol of strontium per cubic km of new crust is used (Ingram et al., 1994) is assumed to
584 be broadly applicable to hydrothermal Sr exchange between seawater and LIPs (Table 3).
585 A doubling of the hydrothermal Sr flux at the onset of OAE 2 (the forcing that is needed
586 to match the $^{87}Sr/^{86}Sr$ data in Fig. 3A) would add 39.9 km^3 of additional new crust
587 production per year on a global scale. Considering the duration of the model perturbation
588 in the hydrothermal Sr flux of 450 kyr, this equates to 15.7 million km^3 of extra basalt
589 production over the duration of OAE 2. The volume of basalts erupted by the Caribbean
590 LIP was estimated by Larson (1991) to be 20.41 million cubic kilometers, indicating that
591 there is enough basalt in the Caribbean LIP to account for the increase in hydrothermal Sr
592 inputs. It seems unlikely that most of the Caribbean LIP (nearly 80%) would have erupted
593 in this relatively short time frame. Larson (1991) documented other LIPs with similar
594 eruption ages that could have also contributed hydrothermal Sr to the oceans, thus
595 increasing the total volume of plateau basalt volcanism to 58.2 million cubic kilometers.
596 Only 27% of this larger volume of LIP basalt would need to erupt in the estimated time
597 frame of 450 kyr.
598 This calculation can provide insight into the likely residence time of Sr in the
599 oceans during the Late Cretaceous and by extension, the Sr concentration of seawater. At
600 higher residence times, a larger perturbation of the hydrothermal Sr flux, and therefore an
601 unreasonably large volume of basalt, would be needed to effect significant changes in
602 seawater $^{87}Sr/^{86}Sr$. This is illustrated by a sensitivity test of varying Sr reservoir sizes (Fig.

603 4) with the Late Cretaceous boundary conditions described in Table 2. For simplicity, the
604 model is forced by an increase in continental weathering of Sr leading up to and during
605 OAE 2, combined with the emplacement of 100% of the estimated volume of the Caribbean
606 LIP erupted over the duration of OAE 2 (Table 3). As shown in Figure 4, as the ocean Sr
607 reservoir size progressively increases, the modeled changes in seawater $^{87}Sr/^{86}Sr$ become
608 smaller, and it becomes increasingly difficult to match the magnitude of the observed
609 decrease in $^{87}Sr/^{86}Sr$ during OAE 2 in the Iona-1 core. Accordingly, at the higher residence
610 times considered in Fig. 4, a larger hydrothermal forcing—and by extension, a volume of
611 basalt greater than the Caribbean LIP—would be required, representing an untenable
612 scenario. In sum, this back-of-the envelope calculation indicates that despite estimates for
613 higher Sr concentrations of Late Cretaceous oceans relative to the modern, which in some
614 calculations are significantly larger by a factor of four to five (e.g., Renard, 1989;
615 Wallmann, 2001; Steuber and Veizer, 2002; Holmden and Hudson, 2003; Coggon et al.,
616 2010; Antonelli et al., 2017), the maximum reasonable Sr residence time is likely to not
617 have been dramatically different.

618 The only way to maintain a high Sr concentration in seawater, and a reasonable
619 oceanic residence time is to increase the throughput of Sr, in the oceans i.e., inputs and
620 outputs of Sr would both have to increase relative to the modern. This could include higher
621 Sr flux inputs from carbonate sources of Sr, including weathering of exposed carbonate
622 platforms in epicontinental marine settings, diagenetic fluxes of Sr from carbonate
623 dissolution, and submarine groundwater discharge in carbonate platform settings
624 (Chaudhuri and Clauer 1986; Huang et al., 2011; Beck et al., 2013; Peucker-Ehrenbrink
625 and Fiske, 2019; Danish et al., 2020), analogous to a process suggested to influence the Ca

626 isotope composition of seawater (Holmden et al., 2012). The main benefit of higher
627 carbonate dissolution fluxes is that there is little effect on the $^{87}Sr/^{86}Sr$ ratio of seawater if
628 the weathered carbonates are, geologically, recently deposited. A second benefit of
629 carbonate weathering is that it introduces the alkalinity that is needed to increase the
630 removal of Sr from the oceans through increased carbonate precipitation rate. Another
631 source of Sr to the oceans that was likely more important in the Cretaceous than it is today,
632 is the submarine weathering of exposed basalt along the flanks of the mid-ocean ridges (cf.
633 Cogné and Humler 2006). As the temperature of ocean bottom waters were much warmer
634 in the Cretaceous (14ºC; Huber et al., 2002) than in present oceans (4ºC), the submarine
635 weathering flux of Sr to the oceans could have been, at its maximum, twice as high as the
636 modern flux (Beck et al., 2013; Peucker-Ehrenbrink and Fiske, 2019). In contrast to the
637 carbonate dissolution/weathering fluxes, which affect the Sr concentration of seawater
638 more than its $^{87}Sr/^{86}Sr$ ratio, low-temperature submarine weathering of basalt by warm
639 ocean bottom waters would drive seawater to higher Sr concentrations (Coogan, 2009;
640 Antonelli et al., 2017) and lower $^{87}Sr/^{86}Sr$ ratios (Ingram et al.,1994; Jones and Jenkyns,
641 2001; Ando et al., 2009)

642 The submarine weathering flux of Sr to the oceans prompts the consideration of
643 additional, but related, assumptions that affects the impact of the validity of the
644 calculations. The first one is that the box model, that is configured for this study, does not
645 allow for any gain or loss of Sr during hydrothermal interactions between seawater and
646 basalt. All Sr from seawater that enters the oceanic crust is exchanged, mole for mole, with
647 basaltic Sr, which is then returned to seawater through venting. This is a common
648 assumption that is made in most ocean Sr box models (Kristall et al., 2017). Recently,

649 Antonelli et al. (2017) demonstrated that secular changes in the Mg and Ca concentrations
650 of seawater affects the Sr exchange capacity of the oceanic crust. For example, the low
651 concentrations of Mg in Cretaceous seawater results in lower fluxes of basaltic derived Sr
652 to the oceans by about 20%, which results in higher predicted $^{87}Sr/^{86}Sr$ ratios for the
653 hydrothermal flux. To account for this effect, a higher $^{87}Sr/^{86}Sr$ ratio of 0.7055 was used in
654 this paper, for the hydrothermal flux of Sr to oceans during OAE 2 (Bickle and Teagle,
655 1992; Kawahata et al., 2001) rather than the more conventional $^{87}Sr/^{86}Sr$ ratio of 0.7025–
656 to 0.7037. The latter range of ratios reflect the modern hydrothermal Sr flux, where all
657 seawater Sr that circulated through the oceanic crust was exchanged for basaltic derived Sr
658 due to the high present day Mg concentration of seawater.
659 While the data in this study support increased continental weathering inputs of Sr,
660 Ca and nutrients to the oceans during OAE 2, the ~1.8-times increase suggested by Sr
661 isotopes is lower than the threefold increase suggested by Ca isotopes (Blättler et al., 2011).
662 The record and interpretation in that study have since been revised by DuVivier et al.
663 (2015). Another study using and δ^7Li as a continental weathering proxy is seemingly in
664 agreement with the original Ca isotope study (Pogge von Strandmann et al., 2013).
665 However, the origin of the negative Li isotope excursion upon which this estimate is based
666 could have multiple interpretations. In fact, the decrease from 20–25‰ before OAE 2, to
667 between 7–10‰ during OAE 2, overlaps δ^7Li values measured in high temperature
668 hydrothermal fluids of 8‰ and in basalt from 5–7 ‰ (Sun et al., 2018). The authors,
669 however, preferred a continental weathering source interpretation that related the change
670 in Li isotopes in marine carbonates to the fractionation of Li isotopes during continental
671 weathering in a period of enhanced (wet) hydrological cycle. In any case, the Li isotope

672 effect is not a small one, and deserves to be followed up with additional study. In the
673 meantime, climate and ocean circulation model studies are needed to examine the effects
674 of the relatively smaller continental weathering flux increase of ~1.8- times found in this
675 study.

676 **7. Conclusions**

677 A high-resolution record of change in the $^{87}Sr/^{86}Sr$ ratio of seawater during OAE 2
678 was reconstructed from the carbonate fraction of the Iona-1 core in the southern WIS.
679 These new $^{87}Sr/^{86}Sr$ data fill in missing details for the $^{87}Sr/^{86}Sr$ seawater curve over this
680 time interval, resolving questions about the timing and magnitude of change in
681 hydrothermal and continental weathering fluxes of Sr to the oceans during OAE 2.
682 Although submarine eruptions of LIPs have been implicated in the decrease in seawater
683 $^{87}Sr/^{86}Sr$ during OAE 2, and other Cretaceous OAEs, for some time, this is the first time
684 that the decrease $^{87}Sr/^{86}Sr$ is shown to have been synchronous with the decrease in the
685 $^{187}Os/^{188}Os$ ratio of seawater, which is the benchmark proxy for tracing massive volcanism
686 during OAE 2. The declining trend in seawater $^{87}Sr/^{86}Sr$ pauses in the middle of OAE 2 for
687 about 150 kyr, which is interpreted to reflect the waning of submarine volcanism at this
688 time, which allows effects of increased continental weathering fluxes of Sr to the oceans
689 to become visible in the record of changing seawater $^{87}Sr/^{86}Sr$ for the first time since onset
690 of OAE 2. An ocean Sr box model was employed simulate the change in seawater $^{87}Sr/^{86}Sr$
691 through OAE 2, and to quantify hydrothermal and continental weathering flux changes.
692 The 1.8-times increase in the continental weathering flux during OEA 2 estimated using Sr
693 isotopes in this study is smaller than threefold increase using Ca and Li isotopes as
694 continental weathering proxies. This lower continental weathering rate has important

ramifications for how OAE 2 and OAEs in general originate and evolve, and what controls nutrient delivery to the oceans during these events.

The modeling and overall conclusions, of this study also hinge on the assumption that the record of changing carbonate $^{87}Sr/^{86}Sr$ ratios in the Iona-1 core accurately records changes in seawater $^{87}Sr/^{86}Sr$ during OAE 2 and immediately before and after OAE 2 as well. The only way to test this assumption is to further examine the Sr record in other marine carbonate OAE 2 successions around the world at the same level of resolution. Finally, a forward model, such as the one employed in this study, helped to explore these relative changes but an inverse model could be used in future work to improve on the estimates presented here.

Acknowledgements

We thank Shell International Exploration and Production Inc. for making samples available. LNY thanks Olivia Wren and Alex Heri for assistance in the laboratory. The manuscript was improved by suggestions of B. Peucker-Ehrenbrink and 2 anonymous reviewers. We also appreciate editorial handling by A. Jacobson. Funding for this project was made possible by National Science Foundation award EAR 1933302 to ADB and KVL and AAPG Student grant in aid and National GEM Consortium fellowship to LNY.

Figures

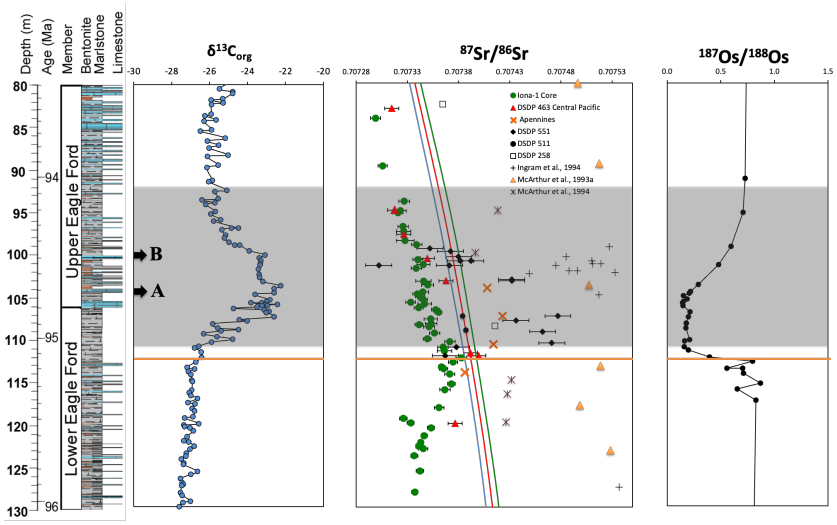

Figure 1: $\delta^{13}C_{org}$ and $^{87}Sr/^{86}Sr$ ratios for samples from the Iona-1 core. The OAE 2 interval is shaded in gray, based on the shift to more positive $\delta^{13}C_{org}$ relative to background values (modified from Eldrett et al., 2014). Os isotope data are from Sullivan et al. (2020). Published $^{87}Sr/^{86}Sr$ data from other locales (McArthur et al., 1993b; 1994; Ingram et al., 1994; Bralower et al., 1997; Frijia and Parante 2008; Ando et al., 2009). The blue, red and green lines represent the seawater $^{87}Sr/^{86}Sr$ minimum, mean and maximum values, respectively, of the LOWESS curve (McArthur et al., 2012). Error bars represent ±2SE uncertainty. The orange line indicates the onset of the shift to less unradiogenic $^{87}Sr/^{86}Sr$ ratios. "A" represents the first inflection point where the massive volcanism at the onset of OAE2 begins waning, as indicated by the rise in $^{187}Os/^{186}Os$ ratios. B is the second inflection point coincident with the decrease of organic carbon burial in ocean sediments, signally a start of the return to pre-excursion $\delta^{13}C_{org.}$

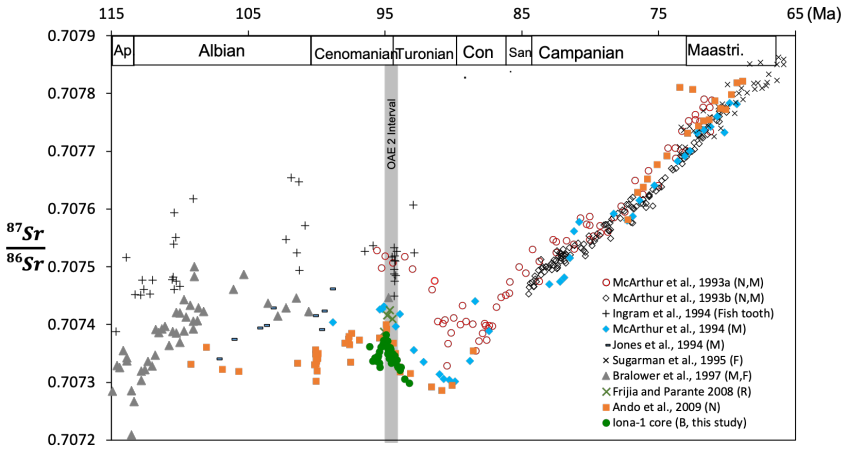

733

734

735

736 **Figure 2:** Compilation of Late Cretaceous $^{87}Sr/^{86}Sr$ data against time (GTS 2020)

737 showing the landscape of changing $^{87}Sr/^{86}Sr$ over time (modified from Ando et al., 2009).

738 All $^{87}Sr/^{86}Sr$ data have been recalibrated to SRM 987 0.710251 (this study). Data from

739 other sources are fitted to the new timescale by simply updating the originally proposed

740 numerical ages for the stage boundaries reported in age model of the paper. F =

741 foraminifera; M = macrofossil; N = nannofossil chalk; R = rudists, B = bulk carbonate

742

743

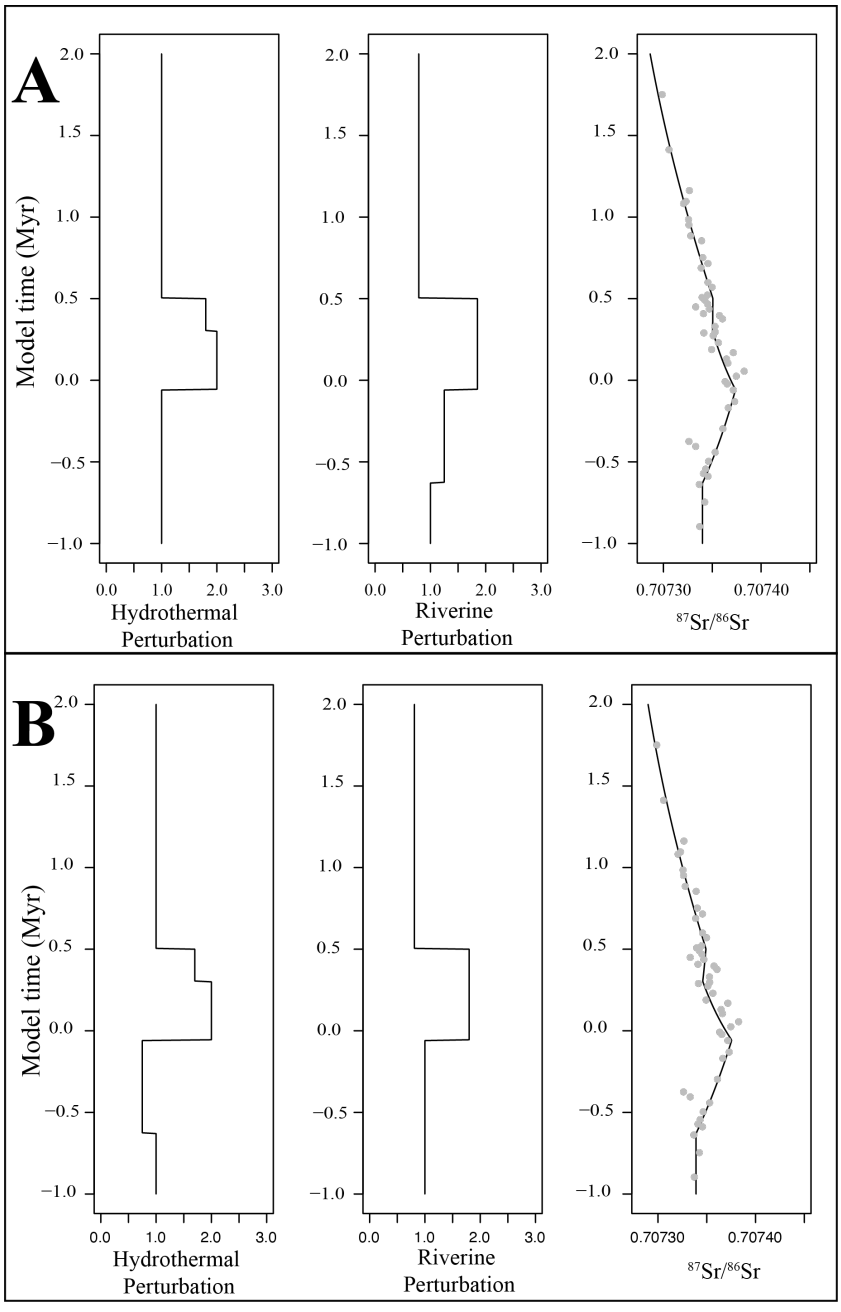
A
B
Model time (Myr)
2.0
1.5
1.0
0.5
0.0
−0.5
−1.0
0.0
1.0
2.0
3.0
Hydrothermal Perturbation
Riverine Perturbation
0.70730
0.70740
$^{87}Sr/^{86}Sr$

744

745
746 **Figure 3:** Box model results of the perturbations in hydrothermal and riverine Sr fluxes
747 needed to simulate the change in seawater $^{87}Sr/^{86}Sr$ ratios during OAE 2 reconstructed
748 using the Iona-1 core. The flux perturbations are normalized to the Sr fluxes that define the
749 pre-OAE 2 steady-state ocean Sr cycle indicted between –1 and –0.65 Myr model-time
750 (Table 2). The LIP eruptions begin at time zero in model-time. The onset of the C-isotope
751 excursion begins 60 kyr later. A.) The increasing trend in seawater $^{87}Sr/^{86}Sr$ before OAE 2
752 is modeled by increasing the continental weathering input Sr flux by 1.25-times. At 0.0
753 Myr, a 2-times increase in the hydrothermal inputs Sr flux and a 1.85-times increase in the
754 continental input Sr flux yields the observed decreasing trend in $^{87}Sr/^{86}Sr$ that begins with
755 the onset of the LIP eruptions. Subsequently, the decreasing trend is arrested for a period
756 of 150 kyr beginning at 0.350 Myr model-time in the record, which is coincident with the
757 evidence for waning volcanism in the seawater Os isotope record. To create the observed
758 change in the slope for this 150 kyr period, the perturbation in the hydrothermal Sr input
759 flux is decreased to 1.8-times and the continental weathering flux Sr input is decreased to
760 0.79 times. This combination of flux changes keeps then seawater $^{87}Sr/^{86}Sr$ decreasing at
761 the end of OAE 2, when the hydrothermal Sr input flux is returned to the pre-OAE 2 values
762 at the end of the peak interval of elevated $\delta^{13}C$ values at 0.5 Myr. B) The increasing trend
763 in seawater $^{87}Sr/^{86}Sr$ before OAE 2 is modeled by decreasing the hydrothermal Sr input
764 flux by 0.75-times. The hydrothermal Sr input flux is increased 2-times, and the continental
765 Sr input flux is increased 1.8-times at the beginning of the LIP eruptions. The 150 kyr
766 interval of no change in seawater $^{87}Sr/^{86}Sr$ is created by decreasing the hydrothermal Sr
767 input flux perturbation to 1.8-times and the continental weathering Sr-flux perturbation to

768 0.81-times. The hydrothermal Sr input flux is returned to the pre-OAE 2 baseline value at

769 the end of the peak interval of elevated $\delta^{13}C$ values.

770
771

772

773

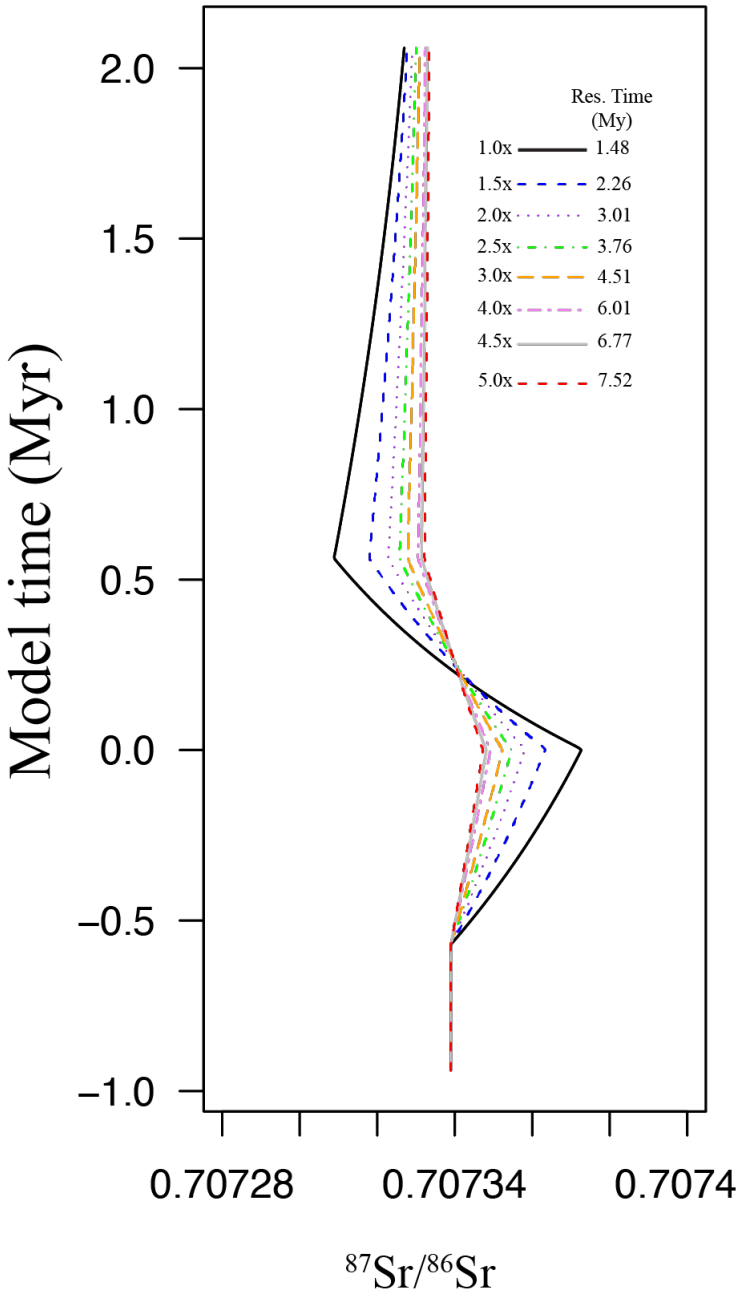
Model time (Myr)
2.0
1.5
1.0
0.5
0.0
−0.5
−1.0
0.70728
0.70734
0.7074
87Sr/86Sr
Res. Time (My)
1.0x 1.48
1.5x 2.26
2.0x 3.01
2.5x 3.76
3.0x 4.51
4.0x 6.01
4.5x 6.77
5.0x 7.52

774

Figure 4: Sensitivity of the box model to the marine residence time of Sr. The residence times reflect increasing the Sr reservoir size relative to the Late Cretaceous boundary conditions (Table 2) up to a residence time of about 7.52 Myr, five times longer than the baseline. The model is forced by increasing continental fluxes (Table 3) and an increase in hydrothermal flux during OAE 2 that is equivalent to the entirety of the Caribbean LIP being emplaced over OAE 2. As the residence time increases, the difference in modeled $^{87}Sr/^{86}Sr$ over OAE 2 becomes progressively smaller. At high residence times, it is impossible to match the decrease in $^{87}Sr/^{86}Sr$ without invoking unreasonable basalt eruption or considering other aspects of the Sr cycle. Onset of OAE 2 is at model time 0

798 **Tables**

799 Table 1: Measured $^{87}Sr/^{86}Sr$ isotope ratios of the Iona-1 core

Stratigraphic height (m)	Age	87Sr /86Sr	2 s.e.
80.25	93.25	0.707299	4.90E-06
85.31	93.59	0.707306	4.46E-06
89.32	93.84	0.707327	5.11E-06
90.57	93.90	0.707323	5.59E-06
90.83	93.92	0.707321	5.07E-06
92.73	94.02	0.707326	5.07E-06
93.44	94.05	0.707326	6.90E-06
94.73	94.12	0.707328	8.80E-06
95.32	94.14	0.707339	5.02E-06
97.41	94.25	0.70734	4.95E-06
98.08	94.28	0.707346	6.28E-06
98.56	94.31	0.707339	5.19E-06
100.30	94.40	0.707346	7.43E-06
100.90	94.43	0.70735	5.94E-06
101.83	94.48	0.707345	5.80E-06
102.21	94.49	0.70734	4.50E-06
102.63	94.51	0.707342	4.44E-06
102.95	94.53	0.707345	4.08E-06
103.33	94.55	0.707333	4.76E-06
103.54	94.56	0.707347	6.85E-06
104.18	94.59	0.707341	4.56E-06
104.44	94.60	0.707357	4.04E-06
104.83	94.62	0.707361	3.18E-06
105.68	94.67	0.707353	6.46E-06
106.45	94.70	0.707353	5.69E-06
106.50	94.71	0.707341	3.88E-06
106.94	94.73	0.707351	5.28E-06
107.82	94.77	0.707356	5.09E-06
108.77	94.81	0.707349	3.85E-06
109.22	94.83	0.707371	4.97E-06

110.01	94.87	0.707365	5.14E-06
110.49	94.90	0.707366	7.09E-06
111.36	94.94	0.707383	5.11E-06
111.88	94.97	0.707375	4.47E-06
112.45	95.01	0.707363	3.03E-06
112.77	95.02	0.707365	3.96E-06
113.42	95.06	0.707372	4.90E-06
114.50	95.13	0.707373	3.75E-06
115.45	95.17	0.707367	5.09E-06
118.16	95.30	0.707361	4.57E-06
119.77	95.37	0.707326	3.66E-06
120.40	95.41	0.707333	3.45E-06
121.09	95.44	0.707353	3.51E-06
122.18	95.50	0.707346	3.01E-06
123.14	95.54	0.707343	2.91E-06
123.68	95.57	0.707341	2.89E-06
124.03	95.59	0.707345	4.45E-06
125.13	95.64	0.707337	3.42E-06
127.31	95.75	0.707342	3.65E-06
130.17	95.90	0.707337	3.14E-06
135.25	96.15	0.707362	6.09E-06

801 Table 2: Comparison of modern ocean Sr budgets with inferred boundary conditions for the OAE 2 models

802

	Modern ocean Sr budget							Late Cretaceous[9] Ocean Sr budget		
	min	Sr	max	min	87Sr/86Sr	max	ref.	change[7]	Sr	87Sr/86Sr	ref.
Reservoir		moles							moles		
Seawater Sr		1.25E+17			0.70918		2		**1.25E+17**	**0.70733**	1
Sr residence time (My)		1.48							1.35		
Sr Fluxes		10^9 mol/y			value or weighted avg.				10^9 mol/y		
global rivers		47.6			0.71107		3				
SGD	7	17.5	28		0.7089		3				
global rivers + SGD	54.6	65.1	75.6		0.71049						
riverine volcanic ash dissolution		1			0.705		3				
eolian volcanic ash dissolution	0.0114	0.017	0.0228		0.705		3				
all continental sources	55.6	66.1	76.6		0.71040				**66.1**	**0.70791**	
diagenetic		5.5			0.70849		3		**5.5**	**0.70733**	
all non hydrothermal Sr inputs	61.1	71.6	82.1		0.71026		3		71.6	0.70786	1
hydrothermal Sr inputs[1]		12.7		0.7025	0.7031	0.7037	3	1.65	**20.9**	**0.7055**	4,5
carbonate precipitation output[8]		84.3					1		**92.5**		1

1. this study; measured or calculated from mass balance
2. Richter et al., (1992)
3. Peucker-Ehrenbrink and Fiske (2019)
4. Bickle and Teagle, 1992, Kawahata et al., 2001
5. Antonelli et al., 2017.
6. Coogan and Dosso (2012)
7. 1.65 times increased sea floor spreading rate; Berner, 1994; 3.8 times increased Sr concentration in the middle Cretaceous oceans (cf. Antonelli et al., 2017)
8. We assume no isotope fractionation occurs during precipitation of CaCO3
9. Bolded values are used in the model simulations of this paper.

803

804

805 Table 3: Calculated volume of oceanic plateau basalt equivalent from the hydrothermal flux during OAE 2

806

	Modern Sr			Doubling the hydrothermal flux			100% eruption of Carrebean LIP		
				Sr Fluxes	10^9 mol/y	$^{87}Sr/^{86}Sr$	Sr Fluxes	10^9 mol/y	$^{87}Sr/^{86}Sr$
	10^9 mol/y	ref.	change[3]						
Continental	66.01	1		Continental	66.01	0.7079	Continental	66.01	0.7079
Hydrothermal	12.70	1	1.65	Hydrothermal	20.96	0.7055	Hydrothermal	20.96	0.7055
				Fraction of total input			Fraction of total input		
Ocean crust production rate	(mol/Km^3)			Continental	0.76		Continental	0.76	
	6.00E+08	2		Hydrothermal	0.24		Hydrothermal	0.24	
				Onset of OAE2[4]	mol/y		Onset of OAE2[4]	mol/y	
Estimated Volume of	Km^3			Hydrothermal	4.19E+01		Hydrothermal	4.82E+10	
Carrebean LIP	2.04E+07	5							
				Crust Production	Km^3		Crust Production	Km^3	
				Background	34.93		Background	34.93	
				Background+LIP	69.85		Background+LIP	80.28	
				LIP	34.93		LIP	45.36	
				Production over OAE2	1.57E+07		Production over OAE2	2.04E+07	
				Fraction of CLIP	0.77		Fraction of CLIP	1.00	

1. Peucker-Ehrenbrink and Fiske (2019)
2. Ingram et al., (1994)
3. 1.65 times increased sea floor spreading rate; Berner, 1994
4. Values used in the model simulations of this paper.
5. Larson 1991

807

808

Field Code Changed

References

Akhtar, A.A., Santi L.M., Griffiths, M.L., Becker, M., Eagle, R.A., Kim, S., Kocsis, L., Rosenthal, Y., and Higgins. J.A. (2020) A record of the $\delta^{44/40}$Ca and [Sr] of seawater Over the last 100 million years from fossil elasmobranch tooth enamel. *Earth Planet. Sci. Lett.* **543**. doi:10.1016/j.epsl.2020.116354.

Andersson P. S., Wasserburg G. J., and Ingri J. (1992) The sources and transport of Sr and Nd isotopes in the Baltic sea. *Earth Planet. Sci. Lett.* **113**, 459–472.

Ando, A., Nakano, T., Kaiho, K., Kobayashi, T., Kokado, E., and Khim B.-K. (2009) Onset of seawater $^{87}Sr/^{86}Sr$ excursion prior to Cenomanian-Turonian oceanic anoxic event 2? New late Cretaceous strontium isotope curve from the central Pacific Ocean: *J. Foram. Res.* **39**, 322–334.

Antonelli M. A., Pester N. J., Brown S. T. and DePaolo D. J. (2017) Effect of paleoseawater composition on hydrothermal exchange in midocean ridges. *Proc. Natl. Acad. Sci.* **114**, 12413–12418.

Bailey, T.R., McArthur, J.M., Prince, H., and Thirlwall, M.F. (2000) Dissolution methods for strontium isotope stratigraphy: whole rock analysis: *Chem. Geol.* **167**, p. 313–319.

Baroni I. R., Topper R. P. M., van Helmond N. A. G. M., Brinkhuis H. and Slomp C. P. (2014) Biogeochemistry of the North Atlantic during ocean anoxic event 2: role of changes in ocean circulation and phosphorus input. *Biogeosciences* **11**, 977–993.

Bennett, V.C., Brandon, A.D., Nutman, A.P. (2007) Coupled ^{142}Nd-^{143}Nd isotopic evidence for Hadean mantle dynamics: *Science* **318**, 1907-1910.

Berner, R. (1994) GEOCARB II: a revised model of atmospheric CO2 levels over Phanerozoic time, *Science* **249**, 1382–1386.

Beck, A.J., Charette, M.A., Cochran, J.K., Gonneea, M.E., Peucker-Ehrenbrink, B. (2013) Dissolved strontium in the subterranean estuary – Implications for the marine strontium isotope budget. *Geochim. Cosmochim. Acta.* **117,** 33–52

Bickle, M.R., Teagle, D.A.H. (1992) Strontium alteration in the Troodos ophiolite: implications for fluid fluxes and geochemical transport in mid-ocean ridge hydrothermal systems. *Earth Planet. Sci. Lett*. **113**, 219–237.

Blättler, C.L., Jenkyns, H.C., Reynard, L.M., and Henderson, G.M. (2011) Significant increases in global weathering during Oceanic Anoxic Events 1a and 2 indicated by calcium isotopes: *Earth Planet. Sci. Lett.* **309**, 77–88.

Bralower, T. J., Fullagar, P. D., Paull, C. K., Dwyer, G. S., and Leckie R. M. (1997) Mid-Cretaceous strontium-isotope stratigraphy of deep-sea sections: *GSA Bull.* **109**, 1421–1442, doi:10.1130/0016-7606(1997)109<1421: MCSISO>2.3.CO;2.

Chaudhuri, S., and Clauer, N. (1986) Fluctuations of isotopic composition of strontium in seawater during the Phanerozoic eon. *Chem. Geol.* **59,** 293–303.

Cochran, J.K., Landman, N.H., Turekian, K.K., Michard, A., Schrag, D.P. (2003) Paleoceanography of the late Cretaceous (Maastrichtian) Western Interior seaway of North America: evidence from Sr and O isotopes. *Palaeogeogr. Palaeoclimatol. Palaeoecol.* **191**, 45–64.

Coggon, R.M., Teagle, D.A.H., Smith-Duque, C.E., Alt, J.C. and Cooper, M.J. (2010) Reconstructing Past Seawater Mg/Ca and Sr/Ca from Mid-Ocean Ridge Flank Calcium Carbonate Veins. *Science* **327,** 1114-1117.

Cogné, J.-P., Humler, E. (2006) Trends and rhythms in global seafloor generation rate. *Geochem. Geophys. Geosyst*. **7**. doi:10.1029/ 2005GC001148.

Coogan L.A. (2009) Altered oceanic crust as an inorganic record of paleoseawatter Sr concentration. Geochem., Geophys., Geosys. 10, Q04001,doi:10.1029/2008GC002341

Coogan, L.A., Dosso, S.E. (2012) An internally consistent, probabilistic, determination of ridge-axis hydrothermal fluxes from basalt-hosted systems. *Earth Planet. Sci. Lett.* **323–324**, 92–101.

Danish, M., Tripathy, G. R., and Rahaman, W. (2020) Submarine groundwater discharge to a tropical coastal lagoon (Chilika lagoon, India): An estimation using Sr isotopes, *Marine Chem.* **224,** 103816. https://doi.org/10.1016/j.marchem.2020.103816.

Demaison, G. J., and Moore G. T. (1980) Anoxic environments and oil source bed genesis, *AAPG Bull.* **64**, 1179–1209.

Derry, L. A., and France-Lanord, C. (1996) Neogene Himalayan weathering history and river 87Sr/86Sr impact on the marine Sr record. *Earth Planet. Sci. Lett.* **142,** 59–74.

Du Vivier, A. D., Selby, D., Sageman, B., Jarvia, I., Grocke, D., and Voigt, S. (2014) Marine $^{187}Os/^{188}Os$ isotope stratigraphy reveals the interaction of volcanism and ocean circulation during Oceanic Anoxic Event 2. *Earth Planet. Sci. Lett.* **389,** 23–33.

Du Vivier A., Jacobson A. D., Lehn G. O., Selby D., Hurtgen M. T. and Sageman B. B. (2015) Ca isotope stratigraphy across the Cenomanian-Turonian OAE 2: Links between volcanism, seawater geochemistry, and the carbonate fractionation factor. *Earth Planet. Sci. Lett.* **416**, 121–131.

El Meknassi S., Dera G., Cardone T., De Rafelis M., Brahmi C., Chavagnac, V. (2018) Sr isotope ratios of modern carbonate shells: Good and bad news for chemostratigraphy. *Geology* **46,** 1003-1006.

902 Elderfield, H. (1986) Strontium isotope stratigraphy. *Palaeogeogr. Palaeoclimatol.*
903 *Palaeoecol.* **57**, 71-90.
904
905
906 Edwards, C.T., Saltzman, M.R., Leslie, S.A., Bergström, S.M., Sedlacek, A.R.C.,
907 Howard, A., Bauer, J.A., Sweet, W.C., and Young, S.A. (2015) Strontium isotope
908 ($^{87}Sr/^{86}Sr$) stratigraphy of Ordovician bulk carbonate: implications for preservation of
909 primary values. *GSA Bull.* **127,** 1275–1289.
910
911 Eldrett, J. S., Minisini, D., and Bergman, S. C. (2014) Decoupling of the carbon cycle
912 during Oceanic Anoxic Event 2. *Geology* **42**, 567–570. doi.org/10.1130/G35520.1
913
914 Eldrett, J. S., Ma, C., Bergman, S. C., Lutz, B., Gregory, F. J., Dodsworth, P., and Kelly,
915 A. (2015a) An astronomically calibrated stratigraphic of the Cenomanian, Turonian and
916 earliest Coniacian from the Cretaceous Western Interior Seaway, USA: Implications for
917 global chronostratigraphy. *Cret. Res.* **56**, 316–344, doi.org/10.1016/j.cretres.2015.04.010.
918
919 Eldrett, J. S., Ma, C., Bergman, S. C., Ozkan, A., Minisini, D., Lutz, B., and Kelly, S. J.,
920 (2015b) Origin of limestone-marlstone cycles: Astronomic forcing of organic rich
921 sedimentary rocks from the Cenomanian to early Coniacian of the Cretaceous Western
922 Interior Seaway, USA. *Earth Planet. Sci. Lett.* **423**, 98–113,
923 doi.org/10.1016/j.epsl.2015.04.026.
924
925 Eldrett, J. S., Dodsworth, P., Bergman, S. C., Wright, M., and Minisini, D. (2017) Water-
926 mass evolution in the Cretaceous Western Interior Seaway of North America and
927 Equatorial Atlantic. *Clim. Past* **13**, 855–878. doi.org/10.5194/cp-13-855-2017.
928
929 Frijia, G., and Parente, M. (2008) Strontium isotope stratigraphy in the upper Cenomanian
930 shallow-water carbonates of the southern Apennines: short-term perturbations of marine
931 $^{87}Sr/^{86}Sr$ during the oceanic anoxic event 2. *Palaeogeogr. Palaeoclimatol. Palaeoecol.* **261**,
932 15–29, doi.org/10.1016/j.palaeo.2008.01.003.
933
934 Hodell D. A., Mead G. A. and Mueller P. A. (1990) Variation in the strontium isotopic
935 composition of seawater (8 Ma to present): implications for chemical weathering rates and
936 dissolved fluxes to the oceans. *Chem. Geol.* **80**, 291–307.
937
938 Holmden C., Muehlenbachs K. and Creaser R. A. (1997a) Depositional environment of the
939 early Cretaceous Ostracode Zone: Paleohydrologic constraints from O, C and Sr isotopes.
940 In, Petroleum Geology of the Cretaceous Mannville Group, Western Canada. Eds. S. G.
941 Pemberton and D. P. James. *Canadian Society of Petroleum Geologists*, **Memoir 18.**
942
943 Holmden, C., Creaser, R.A., Muehlenbachs, K. (1997b) Paleosalinities in ancient brackish
944 water systems determined by $^{87}Sr/^{86}Sr$ ratios in carbonate fossils: a case study from the
945 Western Canada Sedimentary Basin. *Geochim. Cosmochim. Acta* **61**, 2105 – 2118.
946

Holmden C. and Hudson J. D. (2003) $^{87}Sr/^{86}Sr$ and Sr/Ca investigation of Jurassic molluscs from Scotland: Implications for paleosalinities and the Sr/Ca ratio of seawater. *GSA. Bull.* **115,** 1249–1264.

Holmden C., Papanastassiou D. A., Blanchon P. and Evans S. (2012) $\delta^{44/40}Ca$ variability in shallow water carbonates and the impact of submarine groundwater discharge on Ca-cycling in marine environments. *Geochim. Cosmochim. Acta* **83,** 179–194.

Holmden, C., Jacobson, A.D., Sageman, B.B., and Hurtgen, M. (2016) Response of the Cr isotope proxy to Cretaceous Ocean Anoxic Event 2 in a pelagic carbonate succession from the Western Interior Seaway: *Geochim. Cosmochim. Acta*. **186** 277-295. doi/10.1016/j.gca.2016.04.039.

Huang, K.F., You, C.F., Chung, C.H., Lin, I.T. (2011) Nonhomogeneous seawater Sr isotopic composition in the coastal oceans: a novel tool for tracing water masses and submarine groundwater discharge. *Geochem. Geophys. Geosyst.* **12,** 1–14.

Huber, B.T., Norris, R.D., MacLeod, K.G., 2002. Deep-sea paleotemperature record of extreme warmth during the Cretaceous. *Geology* **30,** 123–126.

Ingall, E.D., Bustin, R.M., Van Cappellen, P. (1993) Influence of water column anoxia on the burial and preservation of carbon and phosphorus in marine shales. *Geochim. Cosmochim. Acta* **57 (2)**, 303–316.

Ingall, E. D., and R. Jahnke (1994) Evidence for enhanced phosphorus regeneration from marine-sediments overlain by oxugen depleted waters, *Geochim. Cosmochim. Acta*, **58**, 2571– 2575.

Ingram, B.L., Coccioni, R., Montanari, A., Richter, F.M. (1994) Strontium isotopic composition of mid-Cretaceous seawater. *Science* **264**, 546–550.

Jacobson A. D., Blum J. D., and Walter L. M. (2002) Reconciling the elemental and Sr isotope composition of Himalayan weathering fluxes: Insights from the carbonate geochemistry of stream waters. *Geochimica et Cosmochimica Acta* **66**, 3417-3429.

Jenkyns, H.C. (2010) Geochemistry of oceanic anoxic events. *Geochem. Geophys. Geosyst.* **11**, Q03004, doi:10.1029/2009GC002788.

Jenkyns, H.C., Dickson, A.J., Ruhl, M., van den Boorn, S.H.J.M. (2017) Basalt–seawater interaction, the Plenus Cold Event, enhanced weathering and geochemical change: deconstructing Oceanic Anoxic Event 2 (Cenomanian–Turonian, Late Cretaceous). *Sedimentology* **64,** 16–43

Jones, C. E., and Jenkyns. H. C. (2001) Seawater strontium isotopes, oceanic anoxic events, and seafloor hydrothermal activity in the Jurassic and Cretaceous. *Am. J. Sci.* **301**, 112–149, doi:10.2475/ajs.301.2.112.

Jones, M.M., Sageman, B.B., Selby, D., Jicha, B.R., Singer, B.S., Titus, A.L. (2020) Regional chronostratigraphic synthesis of the Cenomanian-Turonian OAE 2 interval Western Interior Basin (USA): New Re-Os chemostratigraphy and 40Ar/39Ar geochronology, *GSA Bull.* doi.org/10.1130/B35594.1

Kawahata H., Nohara M., Ishizuka H., Hasebe S., Chiba H. (2001) Sr isotope geochemistry and hydrothermal alteration of the Oman ophiolite. *J Geophys Res Solid Earth* **106** 11083–11099.

Kristall B., Jacobson A. D., Hurtgen A. T. (2017) Modeling the paleo-seawater radiogenic Sr isotope record: A case study of the Late Jurassic-Early Cretaceous. *Palaeogeogr. Palaeoclimatol. Palaeoecol.* **472**, 163–176.

Larson, R. L. (1991) Latest pulse of the Earth: Evidence for a mid-Cretaceous superplume, *Geology,* **19,** 547–550.

Leckie, R. M., Bralower, T. J., and Cashman, R. (2002) Oceanic anoxic events and plankton evolution: Biotic response to tectonic forcing during the mid-Cretaceous: *Paleoceanography* **17**, 1041, doi:10.1029/2001PA000623.

Li, D., Shields-Zhou, G.A., Ling, H.F., and Thirlwall, M. (2011) Dissolution methods for strontium isotope stratigraphy: Guidelines for the use of bulk carbonate and phosphorite rocks: *Chem. Geol.* **290**, 133–144, doi:10.1016/j.chemgeo.2011.09.004.

McArthur, J. M., Thirlwall, M. F., Chen, M., Gale, A. S., and Kennedy, W. J. (1993a) Strontium isotope stratigraphy in the late Cretaceous: Numerical calibration of the Sr isotope curve and intercontinental correlation for the Campanian. *Paleoceanography* **8**, 859–873.

McArthur, J. M., Gale, A. S., Kennedy, W. J., Burnett, J. A., Mattey, D., and Lord, A. R., (1993b) Strontium isotope stratigraphy for the Late Cretaceous: a new curve, based on the English chalk, in Hailwood, E. A., and Kidd, R. B. (eds.), *High Resolution Stratigraphy. Geological Society Special Publication* **No. 70**, 195–209.

McArthur, J. M., Kennedy, W. J., Chen, M., Thirlwall, M. F., and Gale, A.S. (1994) Strontium isotope stratigraphy for Late Cretaceous time: Direct numerical calibration of the Sr isotope curve based on the US Western Interior. *Palaeogeogr. Palaeoclimatol. Palaeoecol.* **108**, 95–119.

McArthur, J.M., Howarth, R.J. and Schields, G.A. (2012) Strontium isotope stratigraphy. *in* Gradstein, F.M., Ogg, J.G., Schmitz, M.D. and Ogg, G.M. eds., *The Geologic Time Scale*. Elsevier, Amsterdam, 207– 232.

Minisini, D., Eldrett, J., Bergman, S.C., and Forkner, R. (2017) Chronostratigraphic framework and depositional environments in the organic-rich, mudstone-dominated Eagle Ford Group, Texas, USA. *Sedimentology* **65**, 1520-1557, doi.org/10.1111/sed.12437.

Monteiro, F., Pancost, R., Ridgwell, A., Donnadieu, Y. (2012) Nutrients as the dom-inant control on the spread of anoxia and euxinia across the Cenomanian-Turonian oceanic anoxic event (OAE 2): model–data comparison. *Paleoceanography* **27**, PA4209. https://doi.org/10.1029/2012PA002351.

Montanez, I.P., Banner, J.L., Osleger, D.A., Borg, L.E., and Bosserman, P.J. (1996) Integrated Sr isotope variations and sea-level history of Middle to Upper Cambrian platform carbonates: implications for the evolution of Cambrian seawater $^{87}Sr/^{86}Sr$. *Geology* **24,** 917–920.

Orth C. J., Attrep, Jr., M., Quintana L. R., Elder W. P., Kauffman E. G., Diner R. and Villamil T. (1993) Elemental abundance anomalies in the late Cenomanian extinction interval: a search for the source(s). *Earth Planet. Sci. Lett.* **117**, 189–204.

Owens, J.D., Lyons, T.W., Lowery, C.M. (2018) Quantifying the missing sink for global organic carbon burial during a Cretaceous oceanic anoxic event. *Earth Planet. Sci. Lett.* **499**, 83–94. https://doi.org/10.1016/j.epsl.2018.07.021.

Oxburgh, R. (2001) Residence time of osmium in the oceans. *Geochemistry, Geophys. Geosyst.* **2**, https://doi.org/10.1029/2000GC000104,30

Palmer, M.R., Edmond, J.M. (1989) The strontium isotope budget of the modern ocean. *Earth Planet. Sci. Lett.* **92**, 11–26.

Pedersen, T. F., and Calvert S. E. (1990) Anoxia vs. productivity: What controls the formation of organic-carbon-rich sediments and sedimentary rocks?. *AAPG Bull.* **74**, 454–472.

Peucker-Ehrenbrink, B., and Fiske, G.J. (2019) A continental perspective of the seawater $^{87}Sr/^{86}Sr$ record: a review. *Chem. Geol*. **510**, 140–165.

Pogge von Strandmann, P.A.E., Jenkyns, H.C., and Woodfine, R.G. (2013) Lithium isotope evidence for enhanced weathering during Oceanic Anoxic Event 2. *Nat. Geosci.* **6**, 668–672, doi:10.1038/NGEO1875.

Pratt L., Force E. R., Pomerol B. (1991) Coupled manganese and carbono-isotopic events in marine carbonates at the Cenomnanian-Turonian boundary. *J. Sed. Pet.* **61**, 370–383

Renard, M. (1986) Pelagic carbonate chemostratigraphy (Sr, Mg, $^{18}0$, ^{13}C). *Mar. Micropaleontol.* **10**, 117-164

1084 Richter, F. M., and DePaolo, D. J. (1988) Diagenesis and Sr evolution of seawater using
1085 data from DSDP 590B and 575. *Earth Planet. Sci. Lett.* **90**, 382–394.
1086
1087 Richter, F.M., Rowley, D.B., DePaolo, D. (1992) Sr isotope evolution of seawater: the role
1088 of tectonics. *Earth Planet. Sci. Lett.* **109**, 11–23.
1089
1090 Richter, F.M., Liang, Y. (1993) The rate and consequences of Sr diagenesis in deep-sea
1091 carbonates. *Earth Planet. Sci. Lett.* **117**, 553–565.
1092
1093 Sageman, B.B., Meyers, S.R., Arthur, M.A. (2006) Orbital time scale and new C-isotope
1094 record for Cenomanian–Turonian boundary stratotype. *Geology* **34**, 125–128.
1095
1096 Schlanger, S. O., and Jenkyns, H. C. (1976) Cretaceous oceanic anoxic events: Causes and
1097 consequences: *Geol. Mijnbouw* **55**, 179–184.
1098
1099 Scholle, P. A., and Arthur M. A. (1980) Carbon isotope fluctuations in Cretaceous pelagic
1100 limestones: Potential stratigraphic and petroleum exploration tool. *AAPG Bull.* **64**, 67–87.
1101
1102 Sinton, C. W., and Duncan, R. A., (1997) Potential links between ocean plateau volcanism
1103 and global ocean anoxia at the Cenomanian-Turonian boundary. *Econ. Geol.* **92**, 836–842,
1104 doi:10.2113/gsecongeo.92.7-8.836.
1105
1106 Snow, L. J., Duncan, R. A., and Bralower T. J. (2005) Trace element abundances in the
1107 Rock Canyon Anticline, Pueblo, Colorado, marine sedimentary section and their
1108 relationship to Caribbean plateau construction and oxygen anoxic event 2.
1109 *Paleoceanography* **20**, PA3005, doi:10.1029/2004PA001093.
1110
1111 Steuber T. and Veizer J. (2002) Phanerozoic record of plate tectonic control of seawater
1112 chemistry and carbonate sedimentation. *Geology* **30,** 1123–1126.
1113
1114 Sugarman, P. J., Miller, K. G., Burky, D., and Feigenson, M. D. (1995) Uppermost
1115 Campanian–Maestrichtian strontium isotopic, biostratigraphic, and sequence stratigraphic
1116 framework of the New Jersey Coastal Plain. *GSA Bull.* **107**, 19–37.
1117
1118 Sullivan, D. L., Brandon, A. D., Eldrett, J., Bergman, S. C., Wright, S., and Minisini, D.
1119 (2020) High resolution osmium data record three distinct pulses of magmatic activity
1120 during cretaceous Oceanic Anoxic Event 2 (OAE-2). *Geochim. Cosmochim. Acta* **285**, 257-
1121 273, doi.org/10.1016/j.gca.2020.04.002.
1122
1123 Sun H., Xiao Y. L., Gao Y., Zhang G., Casey J. F. and Shen Y. (2018) Rapid enhancement
1124 of chemical weathering recorded by extremely light seawater lithium isotopes at the
1125 Permian- Triassic boundary. *Proc. Natl. Acad. Sci*. **115**, 3782–3787.
1126
1127 Topper, R. P. M., Trabucho Alexandre, J., Tuenter, E., and Meijer, P. Th. (2011) A regional
1128 ocean circulation model for the mid-Cretaceous North Atlantic Basin: implications for
1129 black shale formation. *Clim. Past* **7**, 277–297, doi:10.5194/cp-7-277-2011.

Trabucho-Alexandre, J., Tuenter, E., Henstra, G.A., van der Zwan, K.J., van de Wal, R.S.W., Dijkstra, H.A., and de Boer, P.L. (2010) The mid-Cretaceous North Atlantic nutrient trap: Black shales and OAEs. *Paleoceanography* **25**, PA4201, doi:10.1029/2010PA001925.

Tribovillard, N., Algeo, T. J., Lyons, T., Riboulleau, A. (2006) Trace metals as paleoredox and paleoproductivity proxies: an update. *Chem. Geol.* **232**, 12−32.

Turgeon, S.C., and Creaser, R.A. (2008) Cretaceous Anoxic Event 2 triggered by a massive magmatic episode. *Nature* **454**, 323–326.

Vérard, C., Hochard, C., Baumgartner, P.O., Stampfli, G.M. (2015) 3Dpalaeogeographic reconstructions of the Phanerozoic versus sea-level and Sr-ratio variations. *J. Palaeogeography* **4**, 64-84.

Veizer, J. (1983) Trace elements and isotopes in sedimentary carbonates, *in* R.J. Reeder ed., Carbonates: Mineralogy and Chemistry. *Reviews in Mineralogy* **11**, 265 300.

Wallmann, K. (2001) Controls on the Cretaceous and Cenozoic evolution of seawater composition, atmospheric CO2 and climate. *Geochim. Cosmochim. Acta* **65,** 3005–3025.

Wickman, F.E. (1948) Isotope ratios: a clue to the age of certain marine sediments. *J. Geol.* **56**, 61–66.

Young, S.A., Saltzman, M.R., Foland, K.A., Linder, J.S., and Kump, L.R. (2009) A major drop in seawater 87Sr/86Sr during the Middle Ordovician (Darriwilian): Links to volcanism and climate?. *Geology,* **37,** 951–954, doi:10.1130/G30152A.1

Zhang, S., and DePaolo,D. J. (2020) Equilibrium calcite-fluid Sr/Ca partition coefficient from marine sediment and pore fluids, *Geochim. Cosmochim. Acta*, **289,** 33-46,